

Finite-temperature Wigner solid and other phases of ripplonic polarons on a helium film

S. N. Klimin¹, J. Tempere^{1,2}, V. R. Misko^{1,3}, and M. Wouters¹

¹*TQC, Universiteit Antwerpen, Universiteitsplein 1, B-2610 Antwerpen, Belgium*

²*Lyman Laboratory of Physics, Harvard University, USA*

³*Departement Fysica, Universiteit Antwerpen, Groenenborgerlaan 171, B-2020 Antwerpen, Belgium*

(Dated: July 9, 2021)

Electrons on liquid helium can form different phases depending on density, and temperature. Also the electron-ripplon coupling strength influences the phase diagram, through the formation of so-called “ripplonic polarons”, that change how electrons are localized, and that shifts the transition between the Wigner solid and the liquid phase. We use an all-coupling, finite-temperature variational method to study the formation of a ripplonpolaron Wigner solid on a liquid helium film for different regimes of the electron-ripplon coupling strength. In addition to the three known phases of the ripplonpolaron system (electron Wigner solid, polaron Wigner solid, and electron fluid), we define and identify a fourth distinct phase, the ripplonpolaron liquid. We analyse the transitions between these four phases and calculate the corresponding phase diagrams. This reveals a reentrant melting of the electron solid as a function of temperature. The calculated regions of existence of the Wigner solid are in agreement with recent experimental data.

I. INTRODUCTION

The two-dimensional (2D) electron system formed on the surface of liquid helium has been widely investigated, especially with regard to the formation and melting of a Wigner crystal, or Wigner solid (WS)¹. In the WS phase, the electrons are self-trapped in a commensurate surface deformation of liquid ⁴He called the dimple lattice^{2–4}. The self-trapping effect of the surface electrons is similar to the formation of polaron states where electrons are dressed by self-induced lattice deformations, or virtual phonons^{5,6}.

Being driven by a force parallel to the surface of liquid ⁴He, the WS moves as a whole keeping the hexagonal order. The electron motion on liquid helium is associated with surface excitations, or ripples (see, e.g.,⁷). When traveling faster than the ripplon phase velocity, as in the case of the Cherenkov radiation, an electron radiates surface waves and the ripples emitted by different electrons interfere constructively if the wave number of the ripples equals the reciprocal lattice vector of the Wigner solid (the Bragg condition). This resonant Bragg-Cherenkov emission of ripples gives rise to the limitation of the electron velocity^{8,9}. Another intriguing nonlinear phenomenon is a sharp rise in mobility at a much higher velocity^{10,11} which was attributed to the *decoupling* of the WS from the dimple lattice. This decoupling can be explained within a hydrodynamic model¹² assuming that the dimple lattice deepens due to the Bragg-Cherenkov scattering which bridges the two above-mentioned phenomena.

One of the most actively developing research directions in the field, which became possible due to the recent advances in the microfabrication technology, is the study of the Wigner solid in confined geometries using devices such as microchannel arrays^{11,15}, single-electron traps¹⁶, field-effect transistors (FET)¹⁷ and charge-coupled devices¹⁸. One of the advances in this direction was ac-

cessing the “quantum wire” regime, when the effective width of a conductive channel is less than the thermal wavelength of the electrons. This was achieved in the recent experiments^{19–22} where the transport properties of electrons were measured in a microchannel with the confinement potential controlled on the scale of the inter-electron separation ($\approx 0.5 \mu\text{m}$). Note that in these experimental studies, electrons are confined in channels with constrictions. In our theoretical model developed for an infinite system we only used typical experimental values of the electron density, n_0 , and the thickness of the helium film (helium depth), h .

The motion of electrons, or in general charged particles, in quasi-one-dimensional (Q1D) channels has been analyzed, using numerical simulations, in early works. For example, the structural, dynamic properties and melting of a Q1D system of charged particles, interacting through a screened Coulomb potential were studied^{23,24} using Monte Carlo simulations. However, the experiments^{19–21} revealed new interesting behavior, such as oscillations in the single-electron conductance in short and long constrictions, which required understanding and therefore stimulated new theoretical and numerical studies. Thus, step-like electric conduction of a classical 2D electron system in a microchannel with a narrow constriction has been analyzed²⁵. Related numerical studies^{26,27}, using molecular-dynamics simulations of Langevin equations of motion of interacting electrons on surface of liquid ⁴He, revealed a significant difference in the electron dynamics for long and short constrictions. The pronounced current oscillations found for a short constriction were shown to be suppressed for longer constrictions^{26,27}, in agreement with the experimental observations. Also, an asymmetric FET-like structure has been proposed²⁷ that allows an easy control of relatively large electron flows and can be used for rectification of an ac-driven electron flow. Furthermore, the authors^{26,27} addressed the important issue of the so-called

“non-sequential ordering of transitions (non-SOT)” characterized by inversions in the subsequent number of electron rows in a Q1D channel, e.g., “1-2-4-3” (see, e.g.,²⁴). In particular, they found the sequence of transitions “1-2-4-3-6-4-5” with two striking inversions “2-4-3” and “3-6-4”²⁷ and demonstrated that some amount of fluctuations (i.e., in the number of particles) restores the usual sequential order, i.e., “1-2-3-4-5”. The role of the potential profile and the form of the interparticle interaction (e.g., the screening length for electrons) in the appearance of the non-SOT has been recently further analyzed in detail^{28,29}.

Despite the above technological, experimental and theoretical advances in the study of the Wigner solid, some of the fundamental properties of this system still remain not well-understood. Moreover, recent experimental studies revealed a number of related issues to be addressed. For example, the experiment²¹ revealed a very gradual increase in the electron effective mass as the temperature drops below the WS transition temperature, while the theory predicted¹² a full formation of dimples at the transition temperature and a very weak temperature dependence. Also, the mechanisms of the decoupling of the Wigner solid from the dimple lattice towards an electron Wigner solid are not yet understood in detail. Also, despite great efforts to observe a bound single-polaron state experimentally, this is still an open problem. The polaronic Wigner crystal is a well-established phenomenon, but the situation for single polarons (which has a particular interest in view of the polaron liquid discussed below) is not yet clear. The work on the observation of a single polaron¹³ was strongly debated.

Here, we analyze in detail various phases of the electron-rippion system, i.e., when the WS is coupled to the dimple lattice, when the WS still exists but is decoupled from the dimple lattice, and when the WS melts, depending on such parameters of the system as the strength of the electron-rippion interaction, temperature and the electron concentration. Also a polaron liquid phase is predicted in the present work at sufficiently high temperatures combined with high coupling strengths. To the best of our knowledge, this phase was not yet considered in the literature. The treatment is performed within the variational scheme similar to that used in Ref.³⁰ for multielectron bubbles in liquid helium.

II. ELECTRON-RIPPLON INTERACTION

The Hamiltonian of a single electron on a flat helium surface is given by

$$\hat{H} = \frac{\hat{\mathbf{p}}^2}{2m} + \sum_{\mathbf{q}} \omega_{\mathbf{q}} \left(\hat{a}_{\mathbf{q}}^+ \hat{a}_{\mathbf{q}} + \frac{1}{2} \right) + \frac{1}{\sqrt{S}} \sum_{\mathbf{q}} V_{\mathbf{q}} (\hat{a}_{\mathbf{q}} + \hat{a}_{-\mathbf{q}}^+) e^{i\mathbf{q}\cdot\mathbf{r}}, \quad (1)$$

where $\hat{\mathbf{p}}$ is the electron momentum operator, m is the electron mass S is the surface area, $\omega_{\mathbf{q}}$ is given by³²,

$$\omega_{\mathbf{q}} = \sqrt{\left(g'q + \frac{\sigma}{\rho} q^3 \right) \tanh(qh)}, \quad (2)$$

where $\sigma \approx 3.6 \times 10^{-4} \text{ J m}^{-2}$ is the surface tension of helium, $\rho = 145 \text{ kg m}^{-3}$ is the mass density of helium, and $g' = g(1 + 3c/\rho gh^4)$ is the acceleration of the liquid due to its van der Waals coupling to the substrate¹⁴ (where g is the acceleration due to gravity and c is the van der Waals coupling of the helium to the substrate). In the Hamiltonian (1), we restrict ourselves to 2D position and momentum operators, assuming that the part of the wave function of the electrons relating to the direction perpendicular to the surface can be factored out exactly. The second-quantization operators $\hat{a}_{\mathbf{q}}^+, \hat{a}_{\mathbf{q}}$ create/annihilate a ripplon with planar wave number \mathbf{q} . The electron-rippion coupling amplitude is given by

$$V_{\mathbf{q}} = \sqrt{\frac{\hbar q}{2\rho\omega_{\mathbf{q}}}} \tanh(qh) eE, \quad (3)$$

where E is the electric field perpendicular to the surface (the so-called ‘pressing field’), e is the electron charge, and h is the thickness of the helium film. The pressing field pushes the electrons with a force eE towards the helium surface. A 1 eV barrier prevents electrons from penetrating the helium surface. The total electric field is a sum of an external (manually applied) field E_{ext} and the electric field induced by the image charge in the substrate with the dielectric constant ε :

$$E = \frac{e^2}{4h^2} \frac{\varepsilon - 1}{\varepsilon + 1} + E_{ext}. \quad (4)$$

It should be noted that the areas of parameters for different phases of a ripplonic polaron system must be determined with a special care on the stability of the system itself. For example, at very high densities, there can exist an instability of the polaron when the pressing field becomes too large³¹. Also there is a maximum surface density of electrons when a uniform distribution is stable on a flat surface⁴⁴.

The self-induced trapping potential of the electron on the helium surface is manifested by the appearance of a dimple in the helium surface underneath the electron, much like the deformation of a rubber sheet when a person is pulled down on it by a gravitational force. The resulting quasiparticle consists of the electron together with its dimple and can be called a ripplonic polaron or ripplonpolaron³³.

The Hamiltonian (1) for the ripplonpolarons is very similar to the Fröhlich Hamiltonian describing polarons³⁴; the role of the phonons is now played by the ripplons. Methods suitable for the study of single polarons have been used to analyze the single polaron on a flat surface^{32,35}. The path integral treatment for a Wigner

solid of polarons has been developed in Refs.^{36,37}. In Ref.³⁰, we adapt their method so that it becomes suitable for the treatment of a lattice of ripplopolarons in multielectron bubbles.

III. HAMILTONIAN FOR A RIPPOPOLARON IN A WIGNER SOLID

In their treatment of the electron Wigner solid embedded in a polarizable medium such as a semiconductors or an ionic solid, Fratini and Qu  merais³⁶ described the effect of the electrons on a particular electron through a mean-field lattice potential. The (classical) lattice potential V_{lat} is obtained by approximating all the electrons acting on one particular electron by a homogenous charge density in which a hole is punched out; this hole is centered in the lattice point of the particular electron under investigation and has a radius given by the lattice distance d . Thus, in their approach, anisotropy effects, e. g., related to the lattice orientation, are neglected. A second assumption implicit in this approach is that the effects of exchange are neglected. This can be justified by noting that for the electrons to form a Wigner solid it is required that their wave function is localized to within a fraction of the lattice parameter as follows from the Lindemann criterion⁴¹.

Within this particular mean-field approximation, the lattice potential can be calculated from classical electrostatics and we find that for a 2D electron gas it can be expressed in terms of the elliptic functions of first and second kind, $E(x)$ and $K(x)$,

$$V_{lat}(\mathbf{r}) = -\frac{2e^2}{\pi d^2} \left\{ |d-r| E \left[-\frac{4rd}{(d-r)^2} \right] + (d+r) \operatorname{sgn}(d-r) K \left[-\frac{4rd}{(d-r)^2} \right] \right\}. \quad (5)$$

Here, \mathbf{r} is the position vector measured from the lattice position. We can expand this potential around the origin to find the small-amplitude oscillation frequency of the electron lattice:

$$\lim_{r \ll d} V_{lat}(\mathbf{r}) = -\frac{2e^2}{d} + \frac{1}{2} m \omega_{lat}^2 r^2 + \mathcal{O}(r^4), \quad (6)$$

with the confinement frequency

$$\omega_{lat} = \sqrt{\frac{e^2}{md^3}}. \quad (7)$$

The ‘phonon’ frequency ω_{lat} of the electron Wigner solid corresponds closely to the longitudinal plasmon frequency that can be derived using an entirely different approach based on a more rigorous study of the modes of oscillations of both the helium surface and the charge distribution on the surface. From this, and from the successful application of this mean-field approach to polaron crystals in solids, we conclude that the approach

based on that of Fratini and Qu  merais describes the influence of the other electrons well in the framework of small amplitude oscillations of the electrons around their lattice point. The phenomenological Lindemann melting criterion⁴¹ suggests that the Wigner solid will melt when the electrons are on average displaced more than a certain value $\delta_0 < 1$ from their lattice position; thus in the regime of interest the Fratini-Qu  merais approach is applicable. In the mean-field approximation, the Hamiltonian for a ripplopolaron in a lattice on a helium surface is given by

$$\hat{H} = \frac{\hat{p}^2}{2m} + V_{lat}(\hat{\mathbf{r}}) + \sum_{\mathbf{q}} \hbar \omega_{\mathbf{q}} \hat{a}_{\mathbf{q}}^{\dagger} \hat{a}_{\mathbf{q}} + \sum_{\mathbf{q}} V_{\mathbf{q}} e^{-i\mathbf{q}\cdot\mathbf{r}} (\hat{a}_{\mathbf{q}} + \hat{a}_{-\mathbf{q}}^{\dagger}). \quad (8)$$

IV. THE RIPPOPOLARON WIGNER SOLID AT FINITE TEMPERATURE

The simple but intuitive approach of the previous section describes the system in the limit of zero temperature. To study the ripplopolaron Wigner solid at finite temperature (and for any value of the electron-ripplon coupling), we use the variational path-integral approach⁴². This variational principle distinguishes itself from Rayleigh-Ritz variation in that it uses a trial action functional S_{trial} instead of a trial wave function.

The action functional of the system described by Hamiltonian (8), becomes, after elimination of the ripplon degrees of freedom,

$$S = -\frac{1}{\hbar} \int_0^{\hbar\beta} d\tau \left\{ \frac{m}{2} \dot{r}^2(\tau) + V_{lat}[r(\tau)] \right\} + \sum_{\mathbf{q}} |V_{\mathbf{q}}|^2 \int_0^{\hbar\beta} d\tau \int_0^{\hbar\beta} d\sigma G_{\omega(\mathbf{q})}(\tau - \sigma) e^{i\mathbf{q}\cdot[\mathbf{r}(\tau) - \mathbf{r}(\sigma)]}, \quad (9)$$

with

$$G_{\nu}(\tau - \sigma) = \frac{\cosh[\nu(|\tau - \sigma| - \hbar\beta/2)]}{\sinh(\beta\hbar\nu/2)}. \quad (10)$$

In preparation of its customary use in the Jensen-Feynman inequality, the action functional (9) is written in imaginary time $t = i\tau$ with $\beta = 1/(k_B T)$ where T is the temperature. Following an approach analogous for a lattice of polarons in an ionic crystal^{36,37}, and to that of Devreese et al. for N polarons in a quantum dot⁴³, we introduce a quadratic trial action of the form

$$S_{trial} = -\frac{1}{\hbar} \int_0^{\hbar\beta} d\tau \left[\frac{m}{2} \dot{r}^2(\tau) + \frac{m\Omega^2}{2} r^2(\tau) \right] - \frac{Mw^2}{4\hbar} \int_0^{\hbar\beta} d\tau \int_0^{\hbar\beta} d\sigma G_w(\tau - \sigma) \mathbf{r}(\tau) \cdot \mathbf{r}(\sigma). \quad (11)$$

where M, w , and Ω are the variationally adjustable parameters. This trial action corresponds to the Lagrangian

$$\mathcal{L}_0 = \frac{m}{2}\dot{r}^2 + \frac{M}{2}\dot{R}^2 - \frac{\kappa}{2}r^2 - \frac{K}{2}(\mathbf{r} - \mathbf{R})^2, \quad (12)$$

from which the degrees of freedom associated with \mathbf{R} have been integrated out. This Lagrangian can be interpreted as describing an electron with mass m at position \mathbf{r} , coupled through a spring with spring constant κ to its lattice site, and to which a fictitious mass M at position \mathbf{R} has been attached with another spring, with spring constant K . The relation between the spring constants in (12) and the variational parameters w, Ω is given by

$$w = \sqrt{K/m}, \quad (13)$$

$$\Omega = \sqrt{(\kappa + K)/m}. \quad (14)$$

Based on the trial action S_{trial} , the Jensen-Feynman variational method allows one to obtain an upper bound for the free energy F of the system (at temperature T) described by the action functional S by minimizing the following function:

$$F_{var} = F_0 - \frac{1}{\beta} \langle S - S_{trial} \rangle_{S_{trial}}, \quad (15)$$

with respect to the variational parameters of the trial action. In this expression, F_0 is the free energy of the trial system characterized by the action S_{trial} , $\beta = 1/(k_b T)$ is the inverse temperature, and the expectation value $\langle S - S_{trial} \rangle_{S_{trial}}$ is to be taken with respect to the ground state of this trial system.

The evaluation of expression (15) is straightforward though lengthy. We find

$$\begin{aligned} F_{var} = & \frac{2}{\beta} \ln \left[2 \sinh \left(\frac{\beta \hbar \Omega_1}{2} \right) \right] + \frac{2}{\beta} \ln \left[2 \sinh \left(\frac{\beta \hbar \Omega_2}{2} \right) \right] \\ & - \frac{2}{\beta} \ln \left[2 \sinh \left(\frac{\beta \hbar w}{2} \right) \right] - \frac{\hbar}{2} \sum_{i=1}^2 a_i^2 \Omega_i \coth \left(\frac{\beta \hbar \Omega_i}{2} \right) \\ & - \frac{\sqrt{\pi} e^2}{\sqrt{D_0}} e^{-d^2/(2D_0)} \left[I_0 \left(\frac{d^2}{2D_0} \right) + I_1 \left(\frac{d^2}{2D_0} \right) \right] \\ & - \frac{1}{2\pi \hbar} \int_0^{k_c} dq q |V_q|^2 \int_0^{\hbar\beta/2} d\tau \frac{\cosh[\omega_q(\tau - \hbar\beta/2)]}{\sinh[\beta \hbar \omega_q/2]} \\ & \times \exp \left[-\frac{q^2}{2} (D_0 - D_\tau) \right]. \end{aligned} \quad (16)$$

In this expression, I_0 and I_1 are Bessel functions of imaginary argument, $k_c = (\rho g'/\sigma)^{1/2}$ is the capillary wave number³². The capillary wave number serves as a cutoff in the integral over q for the polaron free energy. The function D_τ is given by:

$$D_\tau = \frac{\hbar}{m} \sum_{j=1}^2 \frac{a_j^2 \cosh[\hbar \Omega_j (\tau - \beta/2)]}{\Omega_j \sinh(\hbar \Omega_j \beta/2)}, \quad (17)$$

with the coefficients

$$a_1 = \sqrt{\frac{\Omega_1^2 - w^2}{\Omega_1^2 - \Omega_2^2}}; \quad a_2 = \sqrt{\frac{w^2 - \Omega_2^2}{\Omega_1^2 - \Omega_2^2}}. \quad (18)$$

The frequencies Ω_i ($i = 1, 2$) are the eigenfrequencies of the trial system, and w is the third (auxiliary) frequency which is also the variational parameter. The parameter d is the inter-electron distance on the helium surface, which is related to the concentration as:

$$d = \frac{2}{(\sqrt{3}n_0)^{1/2}}.$$

The two first lines in the expression (16) for the variational free energy describe the free energy of the model system and the averaged influence phase of the model system. The third line in (16) is the averaged energy of the Coulomb interaction of the electron with the self-consistent field induced by other electrons. In other words, this is the averaged potential energy of the electron in the Wigner solid. Finally, the last line is the polaron contribution to the free energy.

Optimal values of the variational parameters are determined by numerical minimization of the variational functional F as given by expression (16). The result of the variational path-integral method allows us to introduce different measurable quantities, e. g., temperature to examine the melting of the Wigner solid, and the effective mass of a polaron. The latter one can be estimated as $(m + M)$ where M is the mass of the fictitious particle. A signature of the polaron phase can be a drastic change of the mobility when varying the coupling strength, that can allow one to distinguish between polaron and electron WS experimentally.

V. RESULTS AND DISCUSSION

In this section, we calculate different parameters for a ripplopolaron Wigner solid on the liquid helium surface. This is performed using the variational approach for the polaron free energy as described above. Optimal values of the variational parameters are determined by the numerical minimization of the variational functional F_{var} given by expression (16). We can consider, as a starting point for the treatment, the experimental conditions as obtained from Ref.²⁰, where the thickness of the helium film was $h \approx 1 \mu\text{m}$ to $h \approx 1.7 \mu\text{m}$, the temperature was $T \approx 1 \text{K}$ to $T \approx 1.2 \text{K}$, and the concentration of electrons on the surface was $n_0 \approx 2.58 \times 10^9 \text{cm}^{-2}$ and $n_0 \approx 3.03 \times 10^9 \text{cm}^{-2}$. We however vary temperatures and concentrations in a rather wide range around those values.

The electron-ripplon coupling is measured through the dimensionless coupling constant α determined as³:

$$\alpha = \frac{(eE)^2}{8\pi\sigma} \frac{2m}{\hbar^2 k_c^2}, \quad (19)$$

where E is the electric field applied perpendicular to the surface. It includes both the image field induced by a polar substrate and an external field which can be controlled artificially. Fig. 1 shows the correspondence between E and α for the aforesaid set of material parameters. Note that for $h \approx 1 \mu\text{m}$, the contribution to α from the image field is negligibly small: even with a metallic substrate, $\alpha \gtrsim 10^{-7}$, so that the electron-rippion coupling can be completely controlled by an external field.

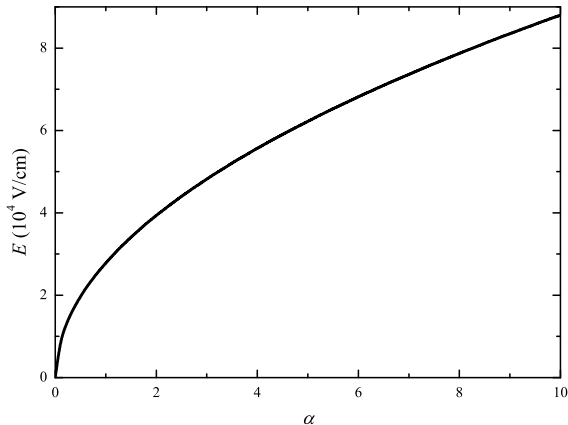


FIG. 1: Dependence of the electric field E measured in V/cm on the dimensionless electron-rippion coupling constant α .

For the numeric calculation, the dimensionless units are used with $\hbar = 1$, the electron mass $m = 1$ and the unit for the energy is $\frac{\hbar^2 k_c^2}{2m} = 1$, where $k_c \approx 6 \times 10^5 \text{ cm}^{-1}$ is the capillary wave number from Ref.³². Also the effective acceleration $g' = 10^8 g$ is taken from Ref.³². Note that, despite a substantial dependence of g' on the helium film thickness, this dependence can only slightly change the phase diagrams calculated below, because at given α , it influences the results only through ripplon frequencies (which are very small for any reasonable g').

The polaronic aspects in the formation of the electron Wigner solid on the liquid helium surface are already thoroughly studied both experimentally and theoretically, see, e. g., the recent review³¹ and references therein. However, some questions remain unexplored. The transition between two types of the Wigner solid (the electron and polaron Wigner solid) at different temperatures is of a particular interest, because this problem requires an arbitrary-coupling finite-temperature polaron theory. We successfully applied this polaron theory to investigate polaron Wigner solids in multielectron bubbles. Here, the same approach is used for the calculation of the phase diagrams on the flat helium surface.

The phenomenological Lindemann criterion⁴¹ is frequently used in the literature for the determination of a melting point in a Wigner solid. This criterion states in general that a crystal lattice of objects (be it atoms, molecules, electrons, or polarons) will melt when the average motion of the objects $\sqrt{\langle \mathbf{r}^2 \rangle}$ around their lattice

site is larger than a critical fraction δ_0 of the lattice parameter d . It would be very hard to calculate from first principles the exact value of the critical fraction δ_0 , but for the particular case of electrons on a helium surface, we can make use of an experimental determination. Grimes and Adams⁴⁵ found that the Wigner solid melts when $\Gamma = 137 \pm 15$, where Γ is the ratio of potential energy to the kinetic energy per electron. In their experiment, the electron density varied from 10^8 cm^{-2} to $3 \times 10^8 \text{ cm}^{-2}$ while the melting temperature T_c varied from 0.23 K to 0.66 K. As estimated in Ref.³⁰ using the experimental data by Grimes and Adams⁴⁵, the critical fraction equals $\delta_0 \approx 0.13$. Recently, a modified Lindemann criterion has been derived in Ref.³¹, which is based on the calculation of a two-site correlation function for the Wigner solid, describing the correlation of displacements for the nearest neighbors. When combined with the Monte Carlo calculation⁴⁶, this leads to the modified value $\delta_0 \approx 0.212$, which is used in the present work. In Ref.³⁰ we used two parallel Lindemann criteria following to the scheme developed in Ref.³⁶. According to this scheme, areas of stability for different phases of a ripplon-polaron system are determined, at least qualitatively, by the parameters $\delta_c \equiv \sqrt{\langle \mathbf{R}_c^2 \rangle} / d$ and $\delta_\rho \equiv \sqrt{\langle \rho^2 \rangle} / d$, where \mathbf{R}_c and ρ are, respectively, the center-of-mass and the relative coordinate for the model polaron system. The averaged squared radii are explicitly determined using the variational parameters for the ripplon-polaron system³⁰,

$$\langle \mathbf{R}_c^2 \rangle = \frac{w^4}{(\Omega_1^2 - \Omega_2^2) [\Omega_1^2 \Omega_2^2 - w^2 (\Omega_1^2 + \Omega_2^2)]^2} \times \left[\frac{\Omega_2^4 (\Omega_1^2 - w^2)}{\Omega_1} \coth \left(\frac{\beta \Omega_1}{2} \right) + \frac{\Omega_1^4 (w^2 - \Omega_2^2)}{\Omega_2} \coth \left(\frac{\beta \Omega_2}{2} \right) \right], \quad (20)$$

$$\langle \rho^2 \rangle = \frac{1}{\Omega_1^2 - \Omega_2^2} \left[\frac{\Omega_1^3}{\Omega_1^2 - w^2} \coth \left(\frac{\beta \Omega_1}{2} \right) + \frac{\Omega_2^3}{w^2 - \Omega_2^2} \coth \left(\frac{\beta \Omega_2}{2} \right) \right]. \quad (21)$$

In principle, four combinations are possible:

(1) The case when both $\delta_c < \delta_0$ and $\delta_\rho < \delta_0$ corresponds to the polaron Wigner solid. In this case, electrons are strongly localized in the Wigner solid together with the dimple lattice on the helium surface. This regime is called in Ref.³¹ the polaron anchoring of the Wigner crystal.

(2) When $\delta_c < \delta_0$ and $\delta_\rho > \delta_0$, the electron Wigner solid exists without anchoring to dimples (electrons leave dimples but the Wigner solid still exists). However, the parameters of this system are still influenced by the electron-phonon interaction through scattering of ripplons on the electrons. Therefore, this regime can be considered as the electron Wigner solid. In other words, this is the Wigner solid of weak-coupling polarons.

(3) When $\delta_c > \delta_0$ and $\delta_\rho < \delta_0$, the ripplonic polarons

are chaotically moving but electrons are in dimples. This case can be interpreted as a polaron liquid. It can be realized when both the coupling strength and the temperature are sufficiently high.

(4) When both $\delta_c > \delta_0$ and $\delta_\rho > \delta_0$, this is the case when the Wigner solid melts to the electron liquid (with the polaron effect).

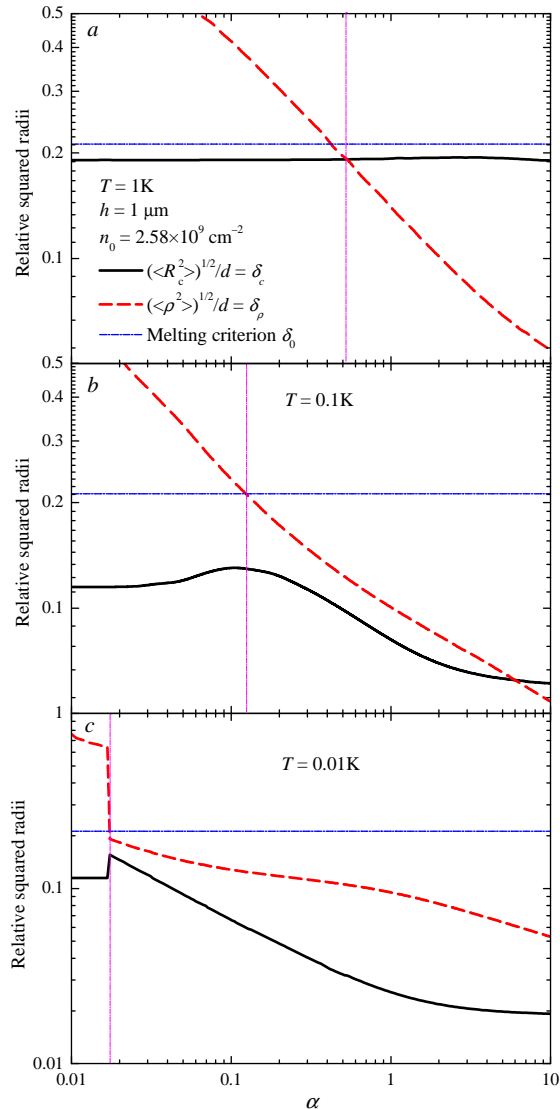


FIG. 2: Parameters δ_c (solid curves) and δ_ρ (dashed curves) for a ripplopolaron Wigner lattice as a function of the coupling constant α for the electron system on the surface of the helium film of the width $h = 1 \mu\text{m}$. The concentration of electrons is $n_0 = 2.58 \times 10^9 \text{ cm}^{-2}$, the temperatures are $T = 1 \text{ K}$ (a), $T = 0.1 \text{ K}$ (b), and $T = 0.01 \text{ K}$ (c). The dot-dashed line shows the critical value $\delta_0 = 0.212$. The vertical lines indicate a transition between polaron and electron Wigner lattices.

In Fig. 2 (a), we plot parameters δ_c (the solid curve) and δ_ρ (the dashed curve) for a ripplopolaron Wigner solid as a function of the coupling constant α for the electron system on the surface of the helium film. The

dot-dashed curve shows the critical value for the modified Lindemann melting criterion $\delta_0 = 0.212$. The thickness of the film is $h = 1 \mu\text{m}$. The concentration of electrons is $n_0 = 2.58 \times 10^9 \text{ cm}^{-2}$, the temperature is $T = 1 \text{ K}$. Under these conditions, the relative averaged squared oscillation amplitude δ_ρ decreases when strengthening the electron-rippolon coupling, passing the critical value δ_c at $\alpha = \alpha_c \approx 0.53$. The center-of-mass relative averaged squared oscillation amplitude, δ_c , varies extremely slightly, being smaller than the critical value at all coupling strengths. In terms of the aforesaid four regimes, this means that the Wigner solid exists at these conditions for all α , changing at $\alpha = \alpha_c$ from the electron Wigner solid at $\alpha < \alpha_c$ to the polaron Wigner solid at $\alpha > \alpha_c$.

In the experiments^{20–22}, where there is no additional external field to enhance α , electrons are attracted to the surface of liquid helium by a rather small image charge. The coupling constant in this regime is small. For example, in the conditions of Ref.²⁰, $\alpha \sim 1.5 \times 10^{-3}$. According to Fig. 2 (a), the ripplopolaron Wigner lattice for small α is stable, thus the result in Fig. 2 (a) is in line with these experiments.

The graphs 2 (a) and (b) show the analogous dependence of the parameters (δ_c, δ_ρ) for lower temperatures: $T = 0.1 \text{ K}$ and $T = 0.01 \text{ K}$, respectively. For a sufficiently low temperature $T = 0.01 \text{ K}$, we can see a sharp transition between two regimes at certain $\alpha \equiv \alpha_c$, which can be qualitatively attributed to a weak and strong-coupling polaron regimes. It was found in Ref.³² that at $T = 0$, there is a crossover between weak-coupling and strong-coupling polaron regimes when varying α . This transition is not discontinuous at non-zero temperatures, although at low temperatures it can be sharp. At $T = 0.01 \text{ K}$, as seen from Fig. 2 (c), this transition is followed by a change of the regime for the Wigner solid: for smaller $\alpha \lesssim \alpha_c$, $\delta_\rho > \delta_0$ and $\delta_c < \delta_0$, so that the Wigner solid is formed by weak-coupling polarons, and for $\alpha \gtrsim \alpha_c$, we see that both δ_c and δ_ρ are smaller than δ_0 , that corresponds to the polaron Wigner solid. At higher temperatures, the crossover between the regimes of electron and polaron Wigner solids is rather smooth. We can see a manifestation of this crossover at $T = 0.1 \text{ K}$ through a non-monotonic dependence of δ_c as a function of the temperature. We can also conclude from the comparison of the behavior of the parameters δ_ρ and δ_c at different temperatures that low temperatures are favorable for the Wigner solid formation and for its polaron anchoring.

Note that we use the same critical value δ_0 for the melting of the Wigner solid and for the polaron dissociation. Only for the former one, there are experimental⁴⁵ and numerical⁴⁶ estimates of the Lindemann criterion, δ_0 , and even these do not agree. However, from Fig. 2 it is clear that a different choice of δ_0 (keeping its range of magnitude) will not change the results qualitatively.

Figure 3 shows the parameters δ_c and δ_ρ for a ripplopolaron Wigner solid at a given coupling strength $\alpha = 1$ as a function of the temperature for the ripplopolaron system

on the surface of the helium film for different electron concentrations. The other parameters are the same as the previous figures. We can see from this figure that both δ_c and δ_ρ increase monotonically when the temperature rises. The parameters δ_ρ and δ_c , pass the critical Lindemann value δ_0 at different temperatures, depending on the electron concentration, so that the transition points between different configurations of the ripplopolaron system depends on the concentration n_0 . For lower n_0 , the transitions between different configurations occurs at lower temperatures.

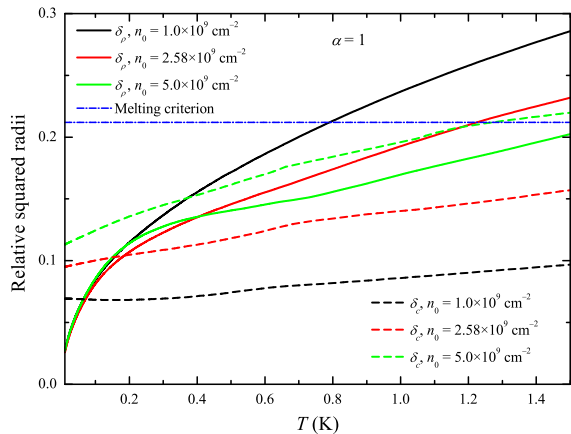


FIG. 3: Parameters δ_c and δ_ρ for a ripplopolaron Wigner lattice as a function of the temperature for the electron system on the surface of the helium film with $\alpha = 1$. The other parameters are the same as in Fig. 2.

In order to obtain a more detailed picture of different regimes for ripplopolaron Wigner solid, we calculate phase diagrams where different regimes for the ripplopolaron system are indicated. Figure 4 contains the phase diagram for the ripplopolaron system on the helium film surface in the variables (T, α) (using the logarithmic scale) calculated for two concentration of electrons $n_0 = 2.58 \times 10^9 \text{ cm}^{-2}$ and $n_0 = 1.0 \times 10^{10} \text{ cm}^{-2}$, and for the thickness of the liquid helium film $h = 1 \mu\text{m}$. In this figure, all four regimes described above can be seen. We can conclude from Fig. 4 that the electron Wigner solid as obtained in the present calculation is expected to be stable at the experimental conditions²⁰, although is rather close to the melting conditions.

It should be noted that the boundary between the regimes with $\delta_c < \delta_0$ and $\delta_c > \delta_0$ corresponds to melting of a Wigner crystal, i. e., this is a true phase transition. On the contrary, the other boundary – between the regimes with $\delta_\rho < \delta_0$ and $\delta_\rho > \delta_0$ indicates a transition between strong-coupling and weak-coupling polaron states. According to the Gerlach-Löwen theorem⁴⁸, there is no phase transition between those regimes for a polaron. At sufficiently high temperatures $T \gtrsim 0.1 \text{ K}$, as shown in³², the transition between strong-coupling and weak-coupling polaron regimes is a crossover rather than

a phase transition. Correspondingly, the transition between the polaron and electron Wigner solids is also a crossover (indicated by grey curves at the figures).

We can see from Fig. 4 that at sufficiently low densities, the melting temperature for the transition between a polaron or electron Wigner solid to a polaron or electron liquid only weakly depends on the electron-rippion coupling constant α , and it becomes more sensitive to α at higher densities. This weak coupling dependence of the melting temperature can be explained by the fact that an overlap of polaron dimples at low densities is relatively small, increasing when rising density. The melting temperature is a non-monotonic function of α , which is one of manifestations of the reentrant melting discussed below.

The other boundary at the phase diagrams in Fig. 4, which corresponds to the polaron dissociation, behaves as follows. When the coupling strength gradually increases at a sufficiently low temperature, the regime of the electron Wigner solid turns at a certain α to the polaron Wigner solid. This critical α rises when increasing temperature. At higher temperatures, when increasing α , the electron liquid can change to the polaron liquid without forming a polaron Wigner solid. It is often assumed that the formation of polaron dimples always leads to their Wigner crystallization. However, according to the present variational calculation, there exists a regime where the polarons are not yet dissociated but their mass is not large enough to form a Wigner crystal. As seen from Fig. 4, it requires a combination of large α and high temperatures. This transition was predicted for an electron-phonon system in a 3D polar crystal³⁶. For a ripplonic polaron system, to the best of our knowledge, this regime was not yet discussed in the literature.

In Fig. 5, we show the phase diagram for the ripplopolaron system on the helium surface in the variables (n_0, α) for two temperatures $T = 0.1 \text{ K}$ and $T = 1 \text{ K}$, keeping other parameters the same as described above. At the lower temperature, we can see in Fig. 5 (a) three regimes for the ripplonic polaron system: the polaron Wigner solid, the electron Wigner solid and the electron liquid. At low temperatures, these three regimes consequently follow each other when increasing the electron concentration. The critical concentration for the transition between the polaron and electron Wigner solids monotonically increases with an increasing coupling strength. The other critical concentration, which indicates melting of the electron Wigner solid into the electron liquid exhibits a non-monotonic behavior as a function of α . At small α , electron-rippion scattering favors the melting of the Wigner crystal, which can be explained by electron-rippion scattering. On the contrary, for larger α the electron-rippion interaction favors the Wigner crystallization because of increase in effective mass of the polarons.

At the higher temperature $T = 1 \text{ K}$, close to the experimental conditions of Ref.²⁰, all four phases of the ripplopolaron system can be observed in the range of densi-

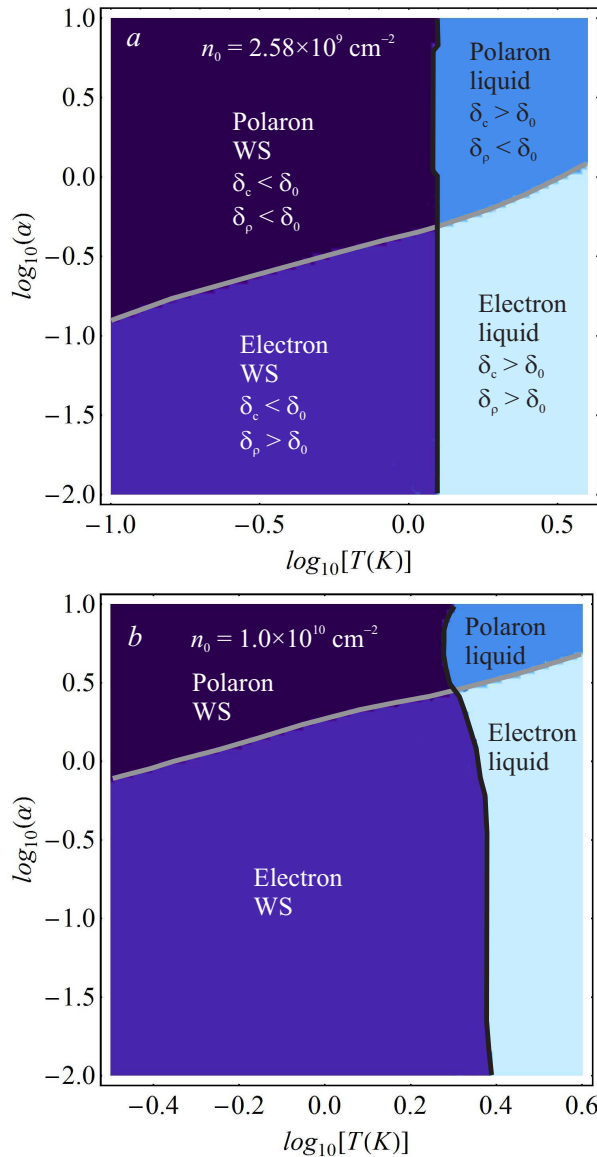


FIG. 4: Phase diagram for the rippolaron system on the helium surface in the variables (T, α) at a concentration of electrons $n_0 = 2.58 \times 10^9 \text{ cm}^{-2}$ (a), $n_0 = 1.0 \times 10^{10} \text{ cm}^{-2}$ (b), for the helium film width $h = 1 \mu\text{m}$.

ties $3 \times 10^7 \text{ cm}^{-2} \lesssim n_0 \lesssim 3 \times 10^{10} \text{ cm}^{-2}$, as seen from Fig. 5 (b). When increasing the coupling strength, the electron liquid can turn into a polaron liquid, and the electron Wigner solid can transform to the polaron Wigner solid, as expected. Remarkably, at the relatively high temperature $T = 1 \text{ K}$, both polaron and electron liquids crystallize, respectively, to polaron and electron Wigner crystals when the electron concentration *increases*, contrary to the low-temperature case. This change of sequence of phases between rippolaron systems at lower and higher temperatures finds a transparent physical explanation through the interplay of the following factors. On one hand, at high temperatures the formation of a

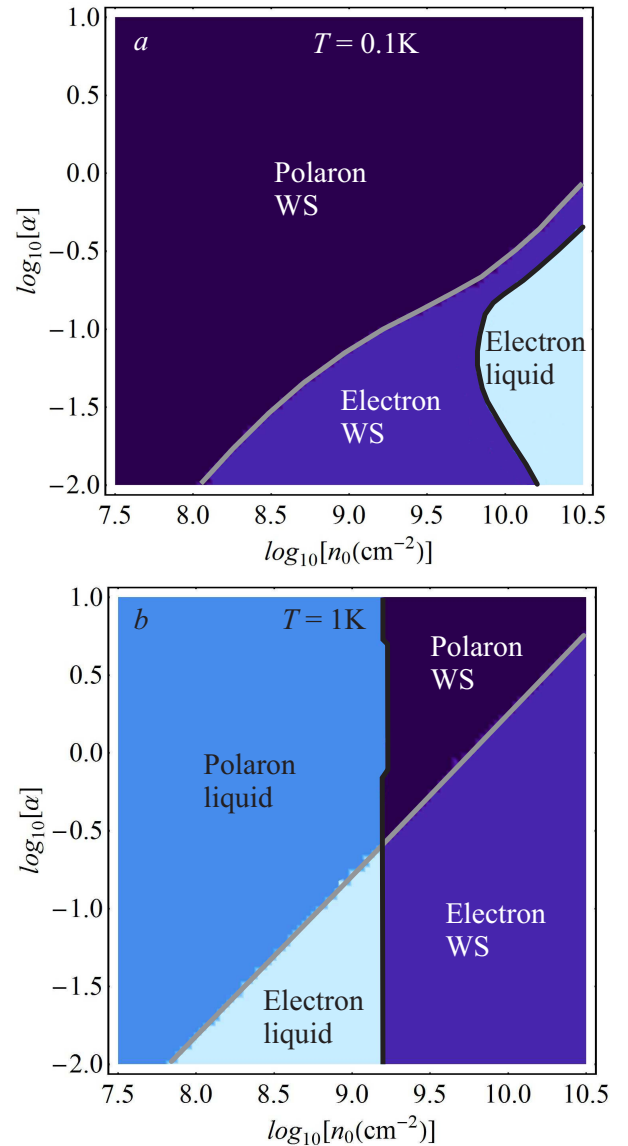


FIG. 5: Phase diagram for the rippolaron system on the helium surface in the variables (n_0, α) for the temperature $T = 0.1 \text{ K}$ (a) and $T = 1 \text{ K}$ (b), with the helium film width $h = 1 \mu\text{m}$.

polaron dimple can be favored by the strengthening of the confinement potential, because the thermal fluctuations of the electron motion become gradually more restricted by the neighboring electrons when decreasing the inter-electron distance. On the other hand, at low temperatures, when thermal fluctuations are less important, melting of the electron Wigner solid can be favored by zero-temperature quantum fluctuations of the electron motion: this is the case of *quantum melting*. We do see quantum melting at nonzero temperature, and it is expected to persist down to $T = 0$. This explains the different sequence of phases between low-temperature and high-temperature regimes for the Wigner solid.

At very high densities, the Fermi energy of electrons can be comparable with their averaged kinetic energy and, consequently, quantum melting of the Wigner crystal can be strongly influenced by the Fermi statistics. Using the material parameters described above, this range of densities is estimated as $n_0 \gtrsim 10^{11} \text{ cm}^{-2}$. In Ref.⁵⁴, quantum melting of an electron WS to a degenerate Fermi gas was experimentally detected at $n_0 \sim 10^{11} \text{ cm}^{-2}$, confirming our estimations. We do not consider here the electron-rippion system at very high densities, when quantum melting occurs to a degenerate Fermi gas. This regime will be a subject of the further study.

Finally, Fig. 6 shows the phase diagram for the riplopolaron system on the helium surface in the variables (n_0, T) plotted using two values of the electron-rippion coupling constant $\alpha = 0.1$ and $\alpha = 0.01$. In analogy with the phase diagrams plotted in Fig. 5, the sequences of different phases when varying the electron concentration and temperature can be described and physically explained in the following way. At small concentrations and low temperatures, the system naturally turns into a polaron Wigner crystal. When increasing the temperature while keeping the concentration constant, the polaron Wigner crystal can either melt to a polaron liquid at low densities, or shed the dimple and change to an electron Wigner crystal at higher densities. In the former case, the breakdown of the polaron Wigner crystal occurs through the melting of the lattice, but polaron dimples survive. In the latter case, the polaron Wigner solid is changed to the electron Wigner solid through the polaron dissociation. When temperature rises further, both the electron Wigner crystal and the polaron liquid can change to the electron liquid but in a different way: the electron Wigner crystal melts, while the polaron liquid dissociates. When increasing the electron concentration at fixed temperature, also the electron Wigner crystal can melt.

Remarkably, the electron liquid phase appears not only for high temperatures but also as an “island” for low temperatures and high electron concentrations (see Figs. 5(a) and 6). This means that the system displays a reentrant melting transition from the electron liquid phase to the electron solid phase at some fixed high n_0 when increasing the temperature or decreasing the coupling strength. In other words, the system displays *solidification by heating* (for high enough electron concentrations). This sort of transition, known as “freezing by heating” transition, has been predicted for mesoscopic systems^{49,50} and recently demonstrated for colloids driven by a non-uniform force⁵¹. This counter-intuitive behavior does not violate principles of thermodynamics and has been observed both in non-equilibrium and equilibrium systems, see, e. g.,^{52,53}.

In Refs.^{49–51}, the mechanism of the inverse melting was explained by the fluctuation-driven increase of the effective size of the particles (i.e., the area effectively occupied by the particle during its fluctuation-driven random motion) in the molten state such that they form a

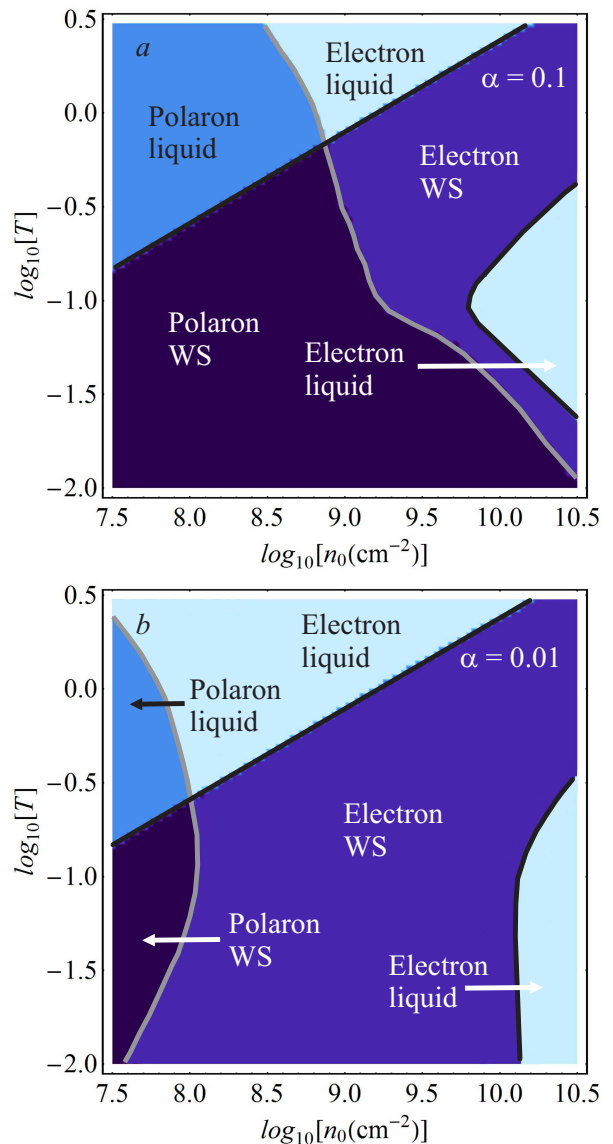


FIG. 6: Phase diagram for the riplopolaron system on the helium surface in the variables (n_0, T) for the coupling strength $\alpha = 0.1$ (a) and $\alpha = 0.01$ (b), with the helium film width $h = 1 \mu\text{m}$.

solid state with increasing temperature. For ripplonic polarons, the revealed sequence of the reentrant electron phases when increasing temperature at high electron concentrations can be explained in other way: by the fact that the melting phase transition is differently driven by quantum and thermal fluctuations. In (20) and (21), *thermal* fluctuations contribute to the temperature dependence of $\langle \mathbf{R}_c^2 \rangle$ and $\langle \rho^2 \rangle$ through the distribution functions $\coth(\beta \hbar \Omega_j / 2)$. The contribution of *quantum* fluctuations to the temperature dependence of the averaged squared radii occurs through the polaron parameters $\{\Omega_j, w\}$ (which also depend on temperature). The electron-rippion interaction can become ef-

fectively stronger with rising temperature in some range of temperatures, and hence the ripplon-induced potential for an electron becomes deeper and narrower in that range. Quantum fluctuations may then favor to a non-monotonic dependence of $\langle \mathbf{R}_c^2 \rangle$ as a function of temperature. On the contrary, thermal fluctuations always contribute to increase $\langle \mathbf{R}_c^2 \rangle$. Thus the transition temperature can result from an interplay of quantum and thermal fluctuations.

When increasing the temperature, the area of the reentrant melting transition shifts to higher concentrations, so that is not seen in Fig. 5(b) but appears in Fig. 5(a). Comparing the phase diagrams for two coupling strengths, we can note that the region of stability for the electron Wigner crystal substantially expands with decreasing α .

As mentioned above, electron-ripplon coupling in the experimental conditions of Refs.²⁰⁻²² (where a stable Wigner crystal has been detected) is rather weak, $\alpha \sim 1.5 \times 10^3$. Hence the obtained phase diagrams are in agreement with these experiments. We can also suggest that the Wigner solid in the experiments²⁰⁻²² can be classified as an electron Wigner solid. For the experiments where the melting point of the electron Wigner lattice at the helium surface was determined using measurements of the mobility and the microwave response^{55,56}, the thickness of the helium film was significantly smaller than in the phase diagrams calculated in the present work. However these experiments are also related to the very weak-coupling polaron regime, where the electron WS rather than the polaron WS can exist.

It should be noted that the film thickness at high densities can be strongly reduced^{57,58}. Consequently, at electron densities of 10^{10}cm^{-2} and higher the helium film can hardly have a thickness $h = 1 \mu\text{m}$. Therefore some portions of the phase diagrams shown in Figs. 4 to 6 are experimentally not accessible. However they represent a theoretical interest for a many-polaron problem.

VI. CONCLUSIONS

In the present work, we have analyzed different phases of a ripplonic polaron system on the surface of a liquid helium film, and the behavior of these phases when varying parameters of the system: the temperature, the electron concentration, and the electron-ripplon coupling strength. The electron-ripplon system is considered in a wide range of electron densities leaving out very high densities where the Fermi statistics becomes important. The treatment has been performed within the arbitrary-coupling and finite-temperature variational path-integral formalism based on the Jensen-Feynman variational principle for the free energy.

We demonstrated that, by varying the electron-ripplon coupling strength α and other parameters such as the electron concentration n_0 on the helium surface and temperature T , in the vicinity of typical experimental val-

ues, the system displays a rich phase behavior. We have found that the experimental conditions corresponding to Ref.²⁰ are favorable for the electron Wigner solid decoupled from the dimple lattice rather than for other phases. This conclusion is in agreement with the observation of an electron Wigner solid in that work.

For a set of typical experimental parameters²⁰⁻²² $h = 1 \mu\text{m}$ and $n_0 = 2.58 \times 10^9 \text{cm}^{-2}$, we revealed four different phases: (i) the electron solid (lattice), at low temperatures and weak couplings; (ii) the polaron Wigner solid, at low temperatures and strong couplings; (iii) the electron liquid, at high temperatures and weak couplings; and (iv) the polaron liquid phase, when the polaron Wigner solid melts but the electrons do not decouple from the dimples, due to the strong electron-ripplon coupling. Remarkably, it should be possible to observe all the predicted phases at typical experimental temperatures close to $T = 1 \text{K}$ ²⁰⁻²², for varying electron concentration and the electron-ripplon coupling strength. For lower temperatures, some of the phases disappear, like the polaron liquid phase.

Thus in addition to three phases of an electron-ripplon system which were studied in the literature, the phase of a *ripplopolaron liquid* is possible at a combination of sufficiently low electron densities, strong electron-ripplon couplings and high temperatures $T \sim 1 \text{K}$. This regime is accessible experimentally, because all these parameters can be controlled, including the coupling strength. Therefore we can expect for an experimental detection of a ripplopolaron liquid.

The system displays even more striking phase behavior when varying the surface electron concentration n_0 and temperature T . For weak electron-ripplon couplings α , the electron liquid phase dominates over a broad range of n_0 and T , although the other above phases can also be observed, like the polaron solid and liquid phases at low electron concentrations. The polaron or electron liquid phase appears at rather high temperatures and can crystallize with increasing n_0 (turning to, respectively, the polaron or electron electron solid). For high electron concentrations, the system exhibits quantum melting accompanied by an unusual reentrant behavior, i.e., the transition from a liquid to solid electron state with *increasing* temperature. This transition is known as the “freezing by heating” transition when fluctuations result in a solidification of a molten state.

The mean-field Wigner approximation used in the present work was successfully applied to polaron Wigner lattices in ionic crystals^{36,37}. The application of this mean-field approach to the WS on a liquid helium surface needs however some care. There exists an enhancement of coupling constant in the Wigner solid phase due to the Bragg scattering of ripples^{3,38,39}. The Bragg scattering of ripples from the electron lattice gives rise to an enhanced deformation of the dimple lattice⁴⁰. This effect can be taken into account, e.g., by introducing an effective Debye-Waller factor in the polaron action (9). The effect of the Bragg scattering can be especially important

at rather weak couplings. It can lead to a quantitative change of the polaron energy and, consequently, to some shift of the boundaries on the phase diagrams. However, it can hardly change the physical picture of phases of the rippopolaron system.

Therefore, we demonstrated the existence of different phases of electrons and polarons on surface of liquid helium, and we analyzed the regions of their stability and the transitions between the revealed phases. Our findings provide a deeper understanding of the phase behavior of the Wigner matter and could be useful for the interpretation of the experimental observations such as the temperature behavior of the decoupling transition (the decoupling of the Wigner solid from the dimples). Furthermore, we expect that the revealed unusual phases (like

polaron liquid) and phase transitions (like the reentrant electron lattice melting) could stimulate further studies, including new experiments.

VII. ACKNOWLEDGEMENTS

We thank A. S. Mishchenko and D. G. Rees for valuable discussions. This research has been supported by the Flemish Research Foundation (FWO-VI), project nrs. G.0115.12N, G.0119.12N, G.0122.12N, G.0429.15N, by the Scientific Research Network of the Research Foundation-Flanders, WO.033.09N, and by the Research Fund of the University of Antwerp.

-
- ¹ *Two-dimensional electron systems on helium and other cryogenic substrates* (ed. E. Y. Andrei, Kluwer Acad. Publ., Dordrecht, The Netherlands, 1997).
 - ² Y. P. Monarkha and V. B. Shikin, *Sov. Phys. JETP* **41**, 710 (1975).
 - ³ D. S. Fisher, B. I. Halperin, and P. M. Platzman, *Phys. Rev. Lett.* **42**, 798 (1979).
 - ⁴ M. Saitoh, *J. Phys. Soc. Jpn.* **55**, 1311 (1986).
 - ⁵ A. S. Alexandrov and J. T. Devreese, *Advances in polaron physics* (Springer, 2010).
 - ⁶ M. I. Dykman and E. I. Rashba, *Physics Today* **68**, 10 (2015).
 - ⁷ J. Tempere, I. F. Silvera, and J. T. Devreese, *Surf. Sci. Rep.* **62**, 159 (2007).
 - ⁸ A. Kristensen, K. Djerfi, P. Fozooni, M. J. Lea, P. J. Richardson, A. Santrich-Badal, A. Blackburn, and R. W. van der Heijden, *Phys. Rev. Lett.* **77**, 1350 (1996).
 - ⁹ M. I. Dykman and Y. G. Rubo, *Phys. Rev. Lett.* **78**, 4813 (1997).
 - ¹⁰ K. Shirahama and K. Kono, *Phys. Rev. Lett.* **74**, 781 (1995).
 - ¹¹ H. Ikegami, H. Akimoto, and K. Kono, *Phys. Rev. Lett.* **102**, 046807 (2009).
 - ¹² W. F. Vinen, *J. Phys. Condens. Matter* **11**, 9709 (1999).
 - ¹³ E. Y. Andrei, *Phys. Rev. Lett.* **52**, 1449 (1984).
 - ¹⁴ G. E. Marques and N. Studart, *Phys. Rev. B* **39**, 4133 (1989).
 - ¹⁵ P. Glasson, V. Dotsenko, P. Fozooni, M. J. Lea, W. Bailey, G. Papageorgiou, S. E. Andresen, A. Kristensen, *Phys. Rev. Lett.* **87**, 176802 (2001).
 - ¹⁶ G. Papageorgiou, P. Glasson, K. Harrabi, V. Antonov, E. Collin, P. Fozooni, P. G. Frayne, M. J. Lea, D. G. Rees, Y. Mukharsky, *Appl. Phys. Lett.* **86**, 153106 (2005).
 - ¹⁷ J. Klier, I. Doicescu, P. Leiderer, *J. Low Temp. Phys.* **121**(5-6), 603-608 (2000).
 - ¹⁸ G. Sabouret, F. R. Bradbury, S. Shankar, J. A. Bert, S. A. Lyon, *Appl. Phys. Lett.* **92**, 082104 (2008).
 - ¹⁹ D. Rees and K. Kono, *J. Low Temp. Phys.* **158**, 301-306 (2010).
 - ²⁰ D. G. Rees, I. Kuroda, C. A. Marrache-Kikuchi, M. Höfer, P. Leiderer, and K. Kono, *Phys. Rev. Lett.* **106**, 026803 (2011).
 - ²¹ D. G. Rees, H. Totsuji, and K. Kono, *Phys. Rev. Lett.* **108**, 176801 (2012).
 - ²² D. G. Rees, H. Ikegami, and K. Kono, *J. Phys. Soc. Jpn.* **82**, 124602 (2013).
 - ²³ G. Piacente, I. V. Schweigert, J. J. Betouras, and F. M. Peeters, *Phys. Rev. B* **69**, 045324 (2004).
 - ²⁴ G. Piacente and F. M. Peeters, *Phys. Rev. B* **72**, 205208 (2005).
 - ²⁵ M. Araki and H. Hayakawa, *Phys. Rev. B* **86**, 165412 (2012).
 - ²⁶ A. A. Vasylenko and V. R. Misko, *Biophys. Rev. Lett.* **9**, 349 (2014).
 - ²⁷ A. A. Vasylenko and V. R. Misko, *Eur. Phys. J. B* **88**, 105 (2015).
 - ²⁸ J. E. Galván-Moya, V. R. Misko, and F. M. Peeters, *Phys. Rev. B* **90**, 094111 (2014).
 - ²⁹ J. E. Galván-Moya, V. R. Misko, and F. M. Peeters, *Phys. Rev. B* **92**, 064112 (2015).
 - ³⁰ J. Tempere, S. N. Klimin, I. F. Silvera, and J. T. Devreese, *Eur. Phys. J. B* **32**, 329 (2003).
 - ³¹ Yu. P. Monarkha and V. E. Syvokon, *Low Temp. Phys.* **38**, 1067 (2012).
 - ³² S. A. Jackson and P. M. Platzman, *Phys. Rev. B* **24**, 499 (1981); *ibid.* **25**, 4886 (1982).
 - ³³ V. B. Shikin and Yu. P. Monarkha, *Zh. Eksp. Teor. Fiz.* **65**, 751 (1973) [*Sov. Phys. JETP* **38**, 373 (1973)].
 - ³⁴ H. Fröhlich, *Advances in Physics* **3**, 325 (1954).
 - ³⁵ S. A. Jackson and F. M. Peeters, *Phys. Rev. B* **30**, 4196 (1984).
 - ³⁶ S. Fratini and P. Quémerais, *Eur. Phys. J. B* **14**, 99 (2000); *ibid.* **29**, 41 (2002).
 - ³⁷ G. Rastelli and S. Ciuchi, *Phys. Rev. B* **71**, 184303 (2005).
 - ³⁸ H. Namaizawa, *Solid State Communications* **34**, 607 (1980).
 - ³⁹ Y. P. Monarkha and K. Kono, *J. Phys. Soc. Japan* **74**, 960 (2005).
 - ⁴⁰ D. G. Rees, N. R. Beysengulov, J.-J. Lin and K. Kono, *Phys. Rev. Lett.* **116**, 206801 (2016).
 - ⁴¹ F. Lindemann, *Z. Phys.* **11**, 609 (1910); C.M. Care and N.H. March, *Adv. Phys.* **24**, 101 (1975).
 - ⁴² R. P. Feynman, *Phys. Rev.* **97**, 660 (1955); R. P. Feynman and A. R. Hibbs, *Quantum Mechanics and Path Integrals* (Mc Graw-Hill, New York, 1965).

- ⁴³ J. T. Devreese, S. N. Klimin, V. M. Fomin, F. Brosens, *Solid State Commun.* **114**, 305 (2000).
- ⁴⁴ L. P. Gor'kov and D. M. Chernikova, *Pis'ma Zh. Eksp. Teor. Fiz.* **18**, 119 (1973) [*JETP Lett.* **18**, 68 (1973)].
- ⁴⁵ C. C. Grimes and G. Adams, *Phys. Rev. Lett.* **42**, 795 (1979).
- ⁴⁶ V. M. Bedanov, G. V. Gadiyak, and Yu. E. Lozovik, *Zh. Eksp. Teor. Fiz.* **88**, 1622 (1985) [*Sov. Phys. JETP* **61**, 967 (1985)].
- ⁴⁷ F. M. Peeters and P. M. Platzman, *Phys. Rev. Lett.* **50**, 2021(1983).
- ⁴⁸ B. Gerlach and H. Löwen, *Rev. Mod. Phys.* **63**, 63 (1991).
- ⁴⁹ D. Helbing, I. J. Farkas, and T. Vicsek, *Phys. Rev. Lett.* **84**, 1240 (2000).
- ⁵⁰ H. E. Stanley, *Nature (London)* **404**, 718 (2000).
- ⁵¹ D. V. Tkachenko, V. R. Misko, and F. M. Peeters, *Phys. Rev. E* **80**, 051401 (2009).
- ⁵² A. L. Greer, *Nature (London)* **404**, 134 (2000); *Journal of the Less-Common Metals* **140**, 327 (1988).
- ⁵³ S.-H. Lee, Y.-C. Lai, C.-H. Du, A. F. Siegenfeld, Y.-J. Kao, P. D. Hatton, D. Prabhakaran, Y. Su, and D.-J. Huang, *Phys. Rev. B* **92**, 205114 (2015).
- ⁵⁴ T. Günzler, B. Bitnar, G. Mistura, S. Nesper, and P. Leiderer, *Surf. Sci.* **361/362**, 831 (1996).
- ⁵⁵ H.-W. Jiang, M. A. Stan, and A. J. Dahm, *Sci.* **196**, 1 (1988).
- ⁵⁶ G. Mistura, T. Günzler, S. Nesper, and P. Leiderer, *Phys. Rev. B* **56**, 8360 (1997).
- ⁵⁷ H. Etz, W. Gombert, W. Idstein, and P. Leiderer, *Phys. Rev. Lett.* **53**, 2567 (1984).
- ⁵⁸ X. L. Hu and A. J. Dahm, *Phys. Rev. B* **42**, 2010 (1990).